geodynamica

Carbon Depletion of Ices by Diamond Precipitation in Sub-Neptune Exoplanets

Albert Zhou [1], **Eric Edmund** [2], **Siegfried H. Glenzer** [1], **Mungo Frost** [*1]

[1] *SLAC National Accelerator Laboratory, Menlo Park, California, USA*
[2] *Institut für Mineralogie, Universität-Münster, Münster, Germany*

Abstract

Hydrocarbons are observed on the surfaces of many icy moons and planets. At high-pressure-high-temperature conditions, such as the ones that occur in large planets, diamond and hydrogen form. Within our solar system, Uranus and Neptune easily reach the required 10 GPa and 2000 K for this process, while icy moons do not. Densities indicative of icy compositions are commonly observed for exoplanets, many of which have radii smaller than Uranus and Neptune icy planets. These so-called 'sub-Neptunes' are a common class of exoplanet and, where hydrocarbons are incorporated within their ices, are candidates for diamond formation. Here, we model icy planets composed of segregated Fe-Si cores, Mg-Si lower mantles and water ice upper mantles in the size range of 0.5 to 1.5 Earth radii. We find that planets above ∼0.75 Earth radii reach diamond formation pressure in their ices, but, in the absence of other heating mechanisms, are only hot enough shortly after their accretion. Where the conditions are met, the denser diamond will sink through the ices deep in the planet under gravity. This provides a source of internal heating and will sequester the carbon deep within the planet. As a consequence, exoplanets with deep ice layers likely have shallow regions depleted in carbon.

Editor(s):
Kate Alyse Waghorn
Richard Garth Gordon
Bernhard Steinberger
Production:
Mohamed Gouiza
Mandy Bethkenhagen

Reviewers:
Anonymous reviewer 1
Anonymous reviewer 2
Anonymous reviewer 3

Submitted:
15 July 2025
Accepted:
24 June 2026
Published:
16 September 2026

1 Introduction

In recent years, the number of known exoplanets has greatly increased. Since the first discovery of exoplanet 51 Peg b (*Mayor and Queloz*, 1995), a large database has been constructed containing close to 6000 bodies with more frequently being discovered, and exoplanets which are smaller and more distant from their host stars becoming possible to detect (*Akeson et al.*, 2013; *Christiansen*, 2018). Despite these advancements, the information available on a particular exoplanet is often limited to its orbital period, mass, and planetary radius (*Baumeister et al.*, 2025).

Knowledge of the mass and planetary radius offers insight into planetary composition via the mean density and reveals various classes of planets (*Rogers and Seager*, 2010). Examples which are not found in our solar system include 'super-Earths'; rocky planets with composition similar to Earth but with larger radii, and 'sub-Neptunes'; planets with lower density consistent with an icy composition and sizes smaller than Uranus or Neptune. Exoplanet compositions are primarily constrained by their mean density, however, this does not uniquely constrain the planetary structure, as different compositions can yield the same mean density. For example, considering a planet with a density consistent with an icy composition and comprising an iron-rich core with layers of rock, ices, and a hydrogen-rich envelope, similar to Uranus and Neptune, the thickness and indeed presence of the layers depend on the thicknesses of the other layers. A thick ice layer could yield the same mean density as a similar planet with a larger high-density core coupled with a thicker hydrogen envelope and much less ice (*Teanby et al.*, 2020).

This uncertainty has led to recent efforts to model possible exoplanet configurations via Markov chain Monte Carlo, Bayesian inference and machine learning techniques (*Spiegel et al.*, 2014; *Dorn et al.*, 2016; *Haldemann et al.*, 2023). Smaller icy planets are of particular interest both from an astrobiology perspective, but also as a class of bodies which do not occur in our solar system, thus less well understood (*Van Hoolst et al.*, 2019; *Tjoa et al.*, 2020). Icy moons, of which there are several in our solar system, exhibit complex and varied chemistry spanning from oxidizing (*Szalay et al.*, 2024; *Frost et al.*, 2025) to reducing (*Loveday et al.*, 2001) conditions, and complex organic molecules are found in their atmospheres and in material ejected from their interiors (*Waite Jr et al.*, 2006; *Hörst*, 2017). This combination of complex carbon chemistry and abundant water makes icy bodies of prominent interest to astrobiology (*Van Hoolst et al.*, 2019; *Tjoa et al.*, 2020).

Recently, it has been discovered that under high-pressure high-temperature conditions, hydrocarbons, which can be held within the ices of moons and planets (*Loveday et al.*, 2001; *Kadobayashi et al.*, 2021), are converted to diamond and a hydrogen-rich phase (*Benedetti et al.*, 1999; *Kraus et al.*, 2017; *Frost et al.*, 2024; *Kadobayashi et al.*, 2021). The demixing of the C-H and C-H-O systems has also been approached using DFT-MD simulations (*Cheng et al.*, 2023; *Roy et al.*, 2025). The diamond is denser than the

*✉ mdfrost@slac.stanford.edu

surrounding ices and will sink due to gravity, leading to the 'diamond rain' phenomenon and providing a source of gravitational heating and convection within the body (*Kraus et al.*, 2017). The conditions required to form diamond are dependent on timescale (*Frost et al.*, 2024; *Schuster et al.*, 2020), but on planetary timescales, it appears that pressures over 10 GPa and temperatures above 2000 K likely suffice (*Benedetti et al.*, 1999; *Kadobayashi et al.*, 2021; *Hirai et al.*, 2009). This has led to discussion of the phenomenon in Uranus and Neptune, where it can affect the internal composition and dynamics (*Benedetti et al.*, 1999; *Kraus et al.*, 2017), which can also be influenced by other phase separation phenomena such as H-water demixing (*Bailey and Stevenson*, 2021; *Bergermann et al.*, 2024; *Cano Amoros et al.*, 2024; *Howard et al.*, 2025), or, in larger planets, H-He demixing (*Howard et al.*, 2024; *Schöttler and Redmer*, 2018). The other icy bodies in the solar system are all moons and too small to generate the required pressures for diamond formation.

Here we seek to address the question of diamond formation from hydrocarbons in icy planets of intermediate sizes between Ganymede, the largest moon in the solar system, in which pressure is too low for diamond formation, and the smaller local icy planet Uranus, which easily meets the conditions needed to form diamond (*Bethkenhagen et al.*, 2017). We focus on small icy planets with sizes is between 0.5 and 1.5 Earth radii and with surface temperatures below 350 K without H/He envelopes. These are smaller than the usual definition of sub-Neptunes, which our results indicate will exceed the size required to reach diamond formation pressures in their ices. Where conditions for diamond precipitation are met within the planetary ices, the conversion of carbon contained within molecules to diamond and its subsequent subduction and sequestration deep within the planet will deplete the surface of carbon. Beyond their average densities, exoplanet compositions can be estimated from the elemental abundances of the host star (*Baumeister et al.*, 2025) and via their atmospheres where spectra can be taken (*Greene et al.*, 2016). Therefore, the sequestration of diamond in icy planet interiors can have a significant influence on the observed bulk carbon content of the planet. The loss of surface carbon will alter the composition of the surface and mantle ices and likely act to inhibit the formation of life, which presumably benefits from abundant organic carbon (*Cockell*, 2020).

2 Methods

Model planets were constructed by self-consistently solving the hydrostatic equilibrium equation and material equations of state. The hydrostatic equilibrium equation is a form of the Adams-Williamson equation and relates the density as a function of radius, $\rho(r)$, and pressure at a given depth, $P(r)$, for a body in hydrostatic equilibrium and has the form:

$$\frac{\mathrm{d}P}{\mathrm{d}r} = -\rho(r)g(r), \quad (1)$$

where $g(r)$ is the acceleration due to gravity at a radius r from the body's center. Here we assume that the planetary composition depends only on the distance from the center and neglect the effect of planetary rotation. Rotation rates and exact compositions likely vary substantially between exoplanets and are poorly constrained, so we consider simplified model planets. The goal is to investigate prototypical planets to establish the overall features required for diamond formation within the planetary ices, rather than to model specific exoplanets.

Our model planets comprise three layers: an iron-rich core at the center, a rocky mantle above the core, and then an upper layer of ices, as shown in Figure 1. As described later, the critical size for a planet to generate sufficient pressure within the ice to support diamond formation is around 0.75 Earth radii. Such a threshold planet would be rather less massive than the Earth due to the lower density of the ice layer. Hydrogen-helium dominated atmospheres are therefore neglected as, unlike Uranus and Neptune, which have substantial hydrogen-rich envelopes, smaller planets are unlikely to sustain such thick atmospheres (*Unterborn and Panero*, 2019). Higher molecular weight atmospheres are possible, but will not add much to the planetary radius, thus, will not affect the results here. For example, the atmospheres of Earth and Venus are only 1-2% of the planet radius.

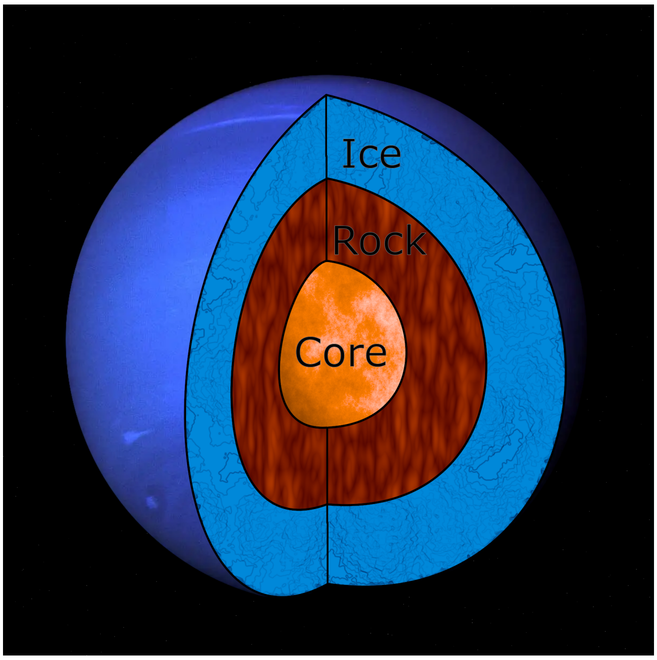

Figure 1 – A cutaway showing the model planetary structure considered in this study. Each layer is assigned a prototypical material equation of state: pure water for the ice; 1:1 Mg:Si magnesium silicates for the rock; and 93 at% Fe-7 at% Si for the core. The thicknesses of each layer are varied to consider different planetary compositions.

To reduce the large degeneracy in the problem space, we make simplifying assumptions about the composition of each of the layers. Planetary cores are believed to be iron-rich with lighter elemental components, reducing the density below that of pure iron (*Spiegel et al.*, 2014; *Bonati et al.*, 2021). Even for Earth, the core composition is not well known (*Hirose et al.*, 2021; *Litasov and Shatskiy*, 2016), and it is not clear how much this will vary between planets. We choose a core comprising 93% Fe and 7% Si as a representative material for which there is an experimental equation of state reaching very extreme pressures (*Wicks et al.*, 2018).

The rocky mantle is composed of magnesium silicates. However, these exhibit large variability in composition with variable Mg to Si ratio and the potential inclusion of other elements. To keep the problem tractable, we fix the composition to be equal parts Mg and Si, based on galactic elemental abundance (*Kobayashi et al.*, 2020). The presence of other ions, for example, Al or Fe (*McDonough and Sun*, 1995), is neglected. Layer mixing, such as might arise from water-rock miscibility (*Dorn and Lichtenberg*, 2021; *Luo et al.*, 2024a; *Kovačević et al.*, 2022), is also omitted. The phases adopted by this stoichiometry and their equations of state are outlined in Table 1.

Finally, we approximate the ice layer to have a density corresponding to pure water. In fact, planetary ices will also contain ammonia (*Naden Robinson et al.*, 2017), methane (*Loveday et al.*, 2001) and other small molecules (*Marboeuf et al.*, 2008), and ions (*Klotz et al.*, 2009). The structures and density of these complex systems are not well understood, and the composition likely varies between planets. Therefore, the equation of state of pure water ice is used, though it should be noted that the inclusion of other materials (*Kadobayashi et al.*, 2020; *Mondal et al.*, 2023), and high temperature (*Haldemann et al.*, 2020; *Lai et al.*, 2023) will generally reduce the density, so this represents an upper bound on the ice density. Details are given in Table 1. To fully explore the problem space, ice thicknesses of 10% to 90% of the planetary radii are considered, corresponding to the definition of 'Hycean worlds' (*Madhusudhan et al.*, 2021). The upper range of this is likely more water-rich than exists for the smaller planets considered here (*Zeng et al.*, 2019; *Rigby and Madhusudhan*, 2024), but is included for completeness.

Our equations of state are based on laboratory measurements and use different functional forms according to the source literature. These are the Vinet equation of state, Equation 2; the 3rd order Birch Murnaghan equation of state, Equation 3; and the Murnaghan equation of state, Equation 4.

$$P = 3B_0 \left(\frac{\rho_0}{\rho}\right)^{-2/3} \left[1 - \left(\frac{\rho_0}{\rho}\right)^{1/3}\right] \times \exp\left\{\frac{3}{2}(B_0' - 1)\left[1 - \left(\frac{\rho_0}{\rho}\right)^{1/3}\right]\right\}, \qquad (2)$$

$$P = \frac{3B_0}{2}\left[\left(\frac{\rho}{\rho_0}\right)^{7/3} - \left(\frac{\rho}{\rho_0}\right)^{5/3}\right] \times \left\{1 + \frac{3}{4}(B_0' - 4)\left[\left(\frac{\rho}{\rho_0}\right)^{2/3} - 1\right]\right\}, \qquad (3)$$

$$P = \frac{B_0}{B_0'}\left[\left(\frac{\rho_0}{\rho}\right)^{-B_0'} - 1\right], \qquad (4)$$

where P is pressure, ρ is density, ρ_0 is the zero-pressure density, B_0 is the zero-pressure bulk modulus, and B_0' is the pressure derivative of the bulk modulus.

The equation of state for the material and phase of interest allows the pressure to be calculated as a function of the density. This can be self-consistently solved with the hydrostatic equilibrium equation, Equation 1, to generate a planet in hydrostatic equilibrium and with the correct material density-pressure relations. The self-consistent solution algorithm is shown graphically in Figure 2.

The planet is divided into 1000 shells of equal thickness. A material is assigned to each shell such that the iron core occupies the center, surrounded by the rocky mantle, and finally the ice layer. Initially, the density is set to the zero-pressure density for each material, and the pressure as a function of radius, $P(r)$, is calculated using the hydrostatic equilibrium equation. The resultant $P(r)$ is then used to calculate a new density profile, $\rho(r)$ using the equation of state for each layer selected according to layer material and pressure. This is compared to the previous $\rho(r)$; if they are within a threshold, set to 10 kg/m^3, the solution is self-consistent and accepted. If they differ, then the new $\rho(r)$ serves as a new best guess to calculate the next iteration of $P(r)$ and the cycle continues.

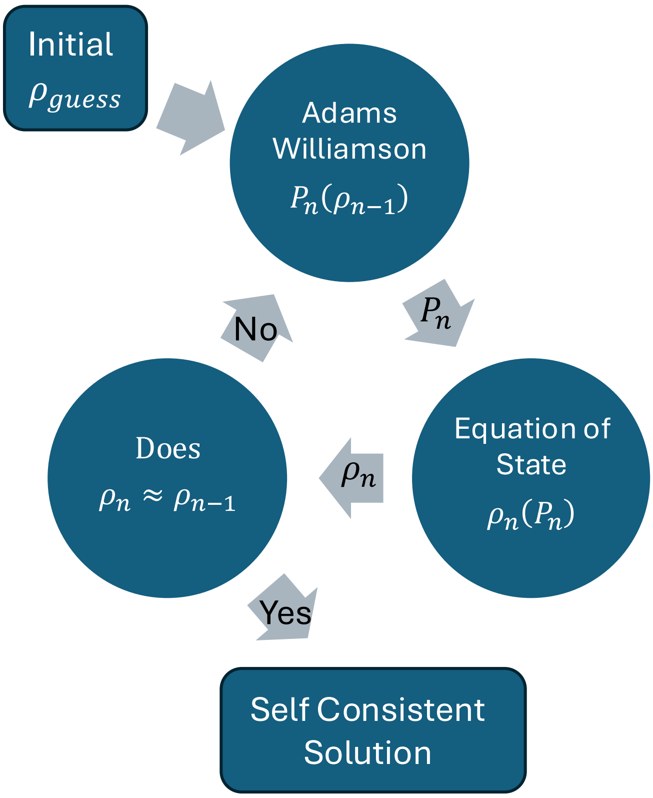

FIGURE 2 – A diagram illustrating the self-consistent solution algorithm used. The initial guess is the zero-pressure density for each material. The hydrostatic equilibrium equation generates the pressure, $P(r)$, within the planet from this density. This $P(r)$ is then used to construct an updated density profile using the material equations of state. The loop continues until the density is unchanged within a threshold of 10 kg/m^3 at which a self-consistent density profile has been generated.

For diamond precipitation to occur from hydrocarbons in the high pressure ices, the pressure in the ice layer must exceed 10 GPa, the formation pressure for diamond from hydrocarbons (*Benedetti et al.*, 1999; *Kadobayashi et al.*, 2021; *Hirai et al.*, 2009). Thus, the planet must be massive enough to generate this pressure and possess sufficiently thick ice layers to reach this pressure within the ices.

Diamond formation also requires temperatures above

Material	Pressure Range (GPa)	$\rho_0(kg/m^3)$	B_0 (GPa)	B'_0	Form	Ref.
Ice Ih	0 to 1.0	930	9.85	6.6	Murnaghan	*Strässle et al.* (2005)
Ice VI	1.0 to 2.1	1271	14.05	4	BM3	*Bezacier et al.* (2014)
Ice VII	>2.1	1456	14.9	5.4	BM3	*Wolanin et al.* (1997)
Forsterite	0 to 14	3221	125	4	BM3	*Downs et al.* (1996)
Wadsleyite	14 to 18	3491	160	4	BM3	*Hazen et al.* (1990)
Ringwoodite	18 to 24	3548	182	4.2	BM3	*Meng et al.* (1994)
Quartz	0 to 2.5	2648	37.4	6.2	BM3	*Wang et al.* (2015)
Coesite	2.5 to 8	2921	96	8.4	BM3	*Levien and Prewitt* (1981)
Stishovite	8 to 24	4290	309.9	4.59	BM3	*Andrault et al.* (2003)
Bridgmanite	24 to 120	4101	256	4	BM3	*Fiquet et al.* (1998)
Post-perovskite	>120	4058	221	4.2	Vinet	*Lin et al.* (2014)
Fe93Si7	All	7678	136.2	5.97	Vinet	*Wicks et al.* (2018)

Table 1 – Equations of state used by material and pressure. The ice layer comprises ice phases (ice Ih, ice VI or ice VII) depending on pressure. The rock layer is an equimolar mixture of Mg_2SiO_4 (forsterite, wadsleyite or ringwoodite) and SiO_2 (quartz, coesite or stishovite) below 24 GPa and $MgSiO_3$ (bridgmanite or post-perovskite) above 24 GPa. The core consists of Fe93Si7. Form refers to the equation of state used, BM3 stands for 3rd order Birch Murnaghan.

2000 K (*Benedetti et al.*, 1999; *Kadobayashi et al.*, 2021; *Hirai et al.*, 2009). The above treatment neglects temperature, as this is poorly constrained and pressure and composition are the dominant controls on mass-radius relations (*Unterborn and Panero*, 2019). Whether a planetary interior will reach the required conditions depends on details of its accretion, evolution, proximity to the host star, and on less well understood effects such as potential runaway greenhouse effects arising from atmospheric water vapor (*Pierrehumbert*, 2023; *Boukrouche et al.*, 2021). The roles of these effects are discussed later.

Adiabatic temperature profiles were constructed using the pressure-radius curves calculated as described above and the AQUA equation of state (*Haldemann et al.*, 2020) for the adiabat. These neglect possible thermal boundary layers (*Deschamps*, 2021) and, thus, are lower bounds on the temperature of mature planets after accretionary heat has dissipated. Temperature of the ices was numerically integrated with the planet surface set to temperatures between 100 K and 350 K. The adiabat for the deeper rock and core layers was not considered.

3 Results and Discussion

3.1 Pressure Within the Ices

Figure 3 shows the result of a Monte Carlo simulation of 20000 model planets. These were constructed with radii between 0.5 and 1.5 Earth radii, focusing on the critical size above which diamond precipitation occurs. These comprise an upper ice layer randomly sampled between 10% and 90% of the total planetary radius with a rocky mantle and iron-rich core of equal thicknesses deeper in the planet. The pressure in the ices can exceed that required for diamond formation in planets larger than ∼0.75 Earth radii, though planets with thinner ice, corresponding to those with higher density, must be larger to reach sufficient compression within the ices. Selected planets and known exoplanets are shown in Figure 3 for comparison.

The most massive planets for a given radius, corresponding to those with the highest density, do not exhibit diamond precipitation conditions within their ices. These planets possess only thin surface ices, which are not sufficiently thick to generate the required 10 GPa under their

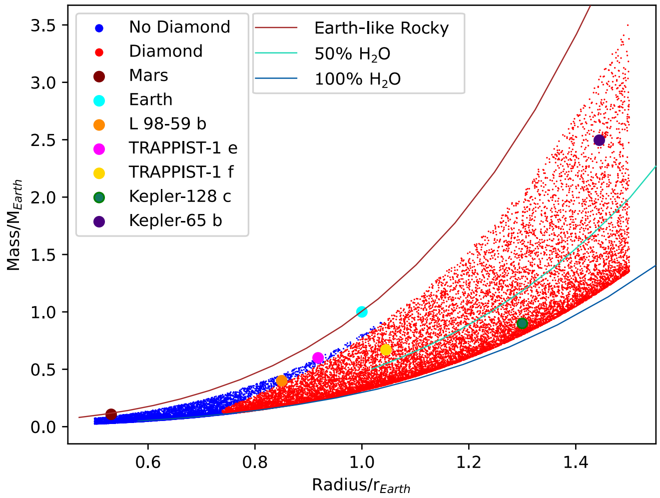

Figure 3 – Monte Carlo sampling of 20000 planets with radii from 0.5 to 1.5 R_{Earth}, ice thickness from 0.1 to 0.9 of the total radius and equal thicknesses of core and rocky mantle. Those in which the pressure exceeds 10 GPa in the ice layer are colored red and meet the pressure requirement for diamond precipitation in the ices, those not meeting this criteria are blue. Select planets and exoplanets are shown by larger points. Planets larger than $\sim 0.75R_{Earth}$ may exhibit diamond precipitation, depending on the thickness of the ice layer. Denser planets require a greater size to generate sufficient pressure within their thin ice layers. Lines show the mass-radius curves for 100% water, 50% water above an Earth-like interior and Earth-like rocky planets from *Zeng et al.* (2019)

own weight. Similarly, in planets near 0.75 Earth radii, close to the smallest size that can exhibit diamond precipitation, the thickness of the ice is critical in dictating whether diamond precipitation pressure is reached. Figure 4 shows the maximal pressure as a function of ice thickness and planetary radius. There is a peak in maximal pressure in the ices where its thickness is ∼50% of the planetary radius. For thinner ice layers, the weight of the ice above is insufficient to generate as much pressure. Counterintuitively, ice thickness above 50% also results in a lower pressure at the bottom of the ice layer. This is due to the reduction in the mass of the core region, which reduces the force of gravity on the ice layer. This competition between the weight of the ice layer exerted from above, and the reduction in the force of gravity acting on the ice layer in the less massive planet results in a larger radius being required for diamond formation in planets with extremely high water contents, compared to those with ice thickness of around 50%.

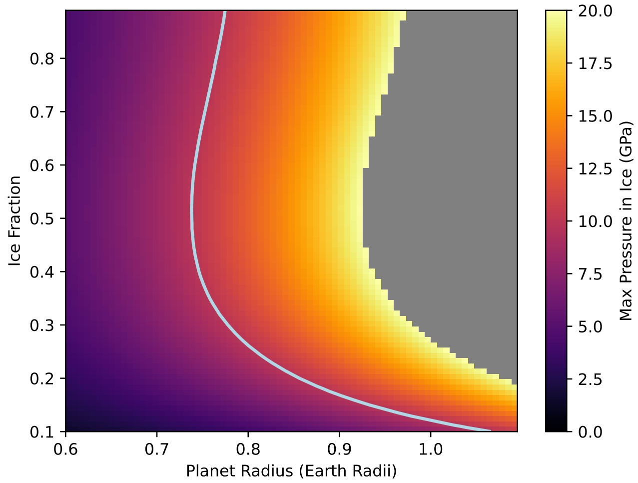

FIGURE 4 – Maximal pressure in the ice layer as a function of ice thickness and planetary radii (equal thicknesses of the core and rocky mantle). The pale blue contour line represents 10 GPa. The gray region indicates pressure greater than 20 GPa.

Figure 5 shows the effect of core to rocky mantle ratio and overall planetary size on the maximal pressure in the ices. For a given planetary radius and ice thickness, a larger core corresponds to greater overall mass and, thus, stronger gravity to compress the ices, which results in higher pressure in the ice layer. Likewise, the stronger gravity of larger planets rapidly increases the reached pressures.

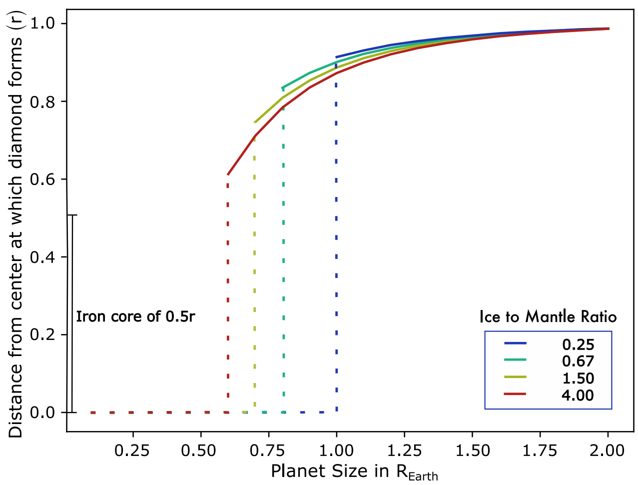

FIGURE 5 – The effect of planetary size and ice portion on the depth at which the ices reach diamond precipitation pressures. Core size is fixed to half of the planetary radius. Line termination at smaller planet sizes indicates the ices do not reach diamond precipitation pressure.

3.2 Discussion of Temperature

Diamond precipitation from hydrocarbons in the ice layers requires both pressures exceeding 10 GPa, as discussed above, and temperatures above 2000 K (*Benedetti et al.*, 1999; *Kadobayashi et al.*, 2021; *Hirai et al.*, 2009). Lower temperature can induce chemical reactions forming more complex hydrocarbons, but will not produce diamond (*Hirai et al.*, 2009; *Kolesnikov et al.*, 2009; *Lobanov et al.*, 2013). The internal temperature will depend on the formation process of the planet, as well as the active mechanisms for heat production and dissipation. Heat dissipation predominantly occurs through radiative, conductive and convective heat transfer. Heat production can occur by various means, such as the decay of radioactive isotopes; tidal heating (*Scharf*, 2006); and gravitational heating, for example, from subduction of denser diamond formed in the ices (*Kraus et al.*, 2017). Heat is also delivered to the planet radiatively, depending on the temperature and proximity of the host star, and by meteor impacts.

The internal temperature profile of exoplanets is a complex topic with substantial ongoing efforts to enable its prediction. It depends on the age, size, composition, and internal dynamics of the planet, as well as its proximity to the host star (*Otegi et al.*, 2020; *Spiegel et al.*, 2014; *Van Hoolst et al.*, 2019). As such, a rigorous treatment covering all possible icy exoplanets is not practical. However, some general features can be discussed by considering specific times after planetary formation. First, we consider the simple case of a fully adiabatic ice layer shown Figure 6.

Figure 6 shows that adiabatic ice layers will not reach sufficient temperature for diamond formation at sizes up to 3 Earth radii. The surface temperature has a strong effect on the internal temperatures of the ices, with warmer surfaces resulting in substantially hotter interiors. Similarly, larger planets for a given surface temperature and composition will have higher temperatures at the base of the ice layer, where both the highest pressure and temperature occur in the ices and so is most conducive to diamond formation. Finally, the thickness of the ice layer has a weaker effect on the temperature at its base. However, layers thinner than 30% of the planetary radius reach lower temperatures due to lower pressure. Conversely, ice thickness over ∼30% of the planetary radius also results in a lower maximal temperature. This is due to the reduced overall mass of the planet resulting in weaker gravity and lower pressure gradients within the ices, as well as lower maximal pressure at the base of the ice layer, Figure 4.

An adiabatic interior makes temperature the limiting factor for diamond formation. However, there are specific times in planetary development where temperatures are much higher. Next, we consider a time shortly after planetary accretion and the differentiation of the core, rocky mantle, and ices, and then effects which can occur later in its lifetime, such as continued radioactive heating, tidal heating, and greenhouse effects.

High temperatures, and hence diamond formation, are expected shortly after the planet forms and has undergone differentiation, forming the core, rock, and ice layers. Young planets are hot from residual energy from planetary accretion, for example, it is believed that the Earth was fully molten after its formation (*Elkins-Tanton*, 2012). The degree of heating is a complex subject and depends on the model used and the nature of the accretion, the velocity and mass distributions of the accreting material, details of the impact events, and on thermal transport within the

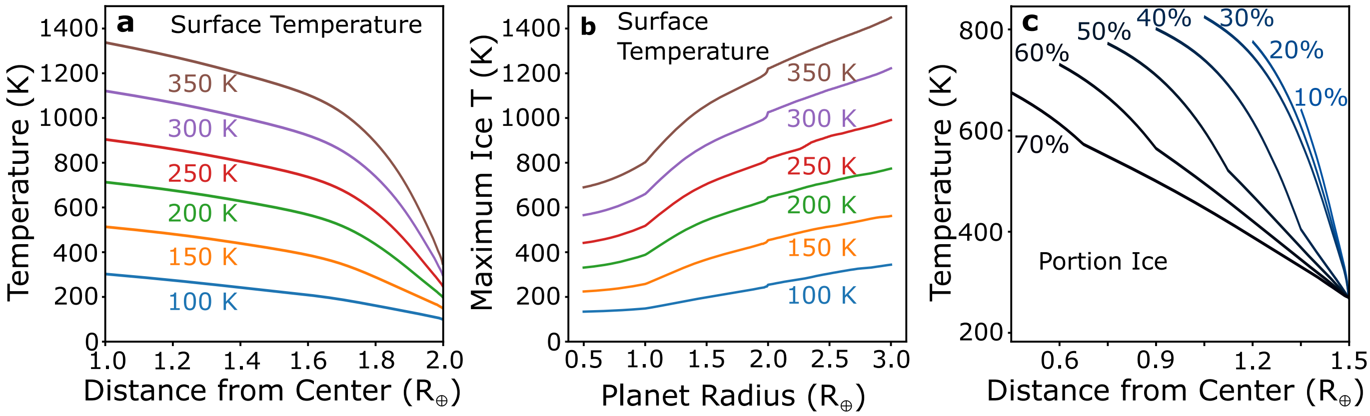

Figure 6 – Adiabatic temperature profiles in the ice layer. **a**: A 2 Earth radius planet consisting of an ice layer thickness 1 Earth radius and equal depths of rock and core material below with various surface temperatures, as indicated. Hotter surfaces result in higher internal temperatures. **b**: The maximum temperature in the ice layer, corresponding to its base, of planets with half their radii of ice thickness and equal depths of rock and core below for various surface temperatures. Larger planets have hotter ices. **c**: Temperature profiles for 1.5 Earth radius planets with ice thicknesses of the marked portion of the total radius and equal depths of rock and core. Note the maxima in the ice temperature occurs for planets with ice layers around 30% of the planetary radius.

planetary embryo. Such models suggest that Earth and Mars-sized planets will easily reach 2000 K in their upper mantles (*Horedt*, 1980; *Elkins-Tanton*, 2012; *Schubert and Spohn*, 1990). The critical mass and radii for icy planets to achieve sufficient pressure for diamond precipitation in their ices are in this size range (Figure 3). Therefore, it is likely that icy planets meeting the pressure criteria for diamond formation are also hot enough shortly after accretion for it to occur.

The separation of planetary embryos into layers via differentiation and accretion occurs concurrently, and young planets are subject to the greatest heating from impact events, which are more frequent early in a planet's existence. Larger impact events contribute more energy to a planet as the heat is deposited deep within them, preferentially heating the upper layers (*Ransford*, 1982). Smaller impacts deposit their energy at the surface, where it can be quickly radiated into space. Thus, a late heavy bombardment (*Bottke and Norman*, 2017) could lead to substantial heating of the ices. This is concurrent with the period of strongest radioactive heating early in a planet's lifespan (*Hanks and Anderson*, 1969). Substantial diamond formation and subsequent sequestration of the carbon deeper within the planet are therefore expected early in planetary development.

Carbon is also delivered to planets after formation, for example, in the form of carbonaceous chondrites (*Pearson et al.*, 2006). It has been proposed that a substantial portion of the Earth's carbon budget was received as a late veneer after the bulk of planetary formation and bombardment was complete (*Wang and Becker*, 2013). The thermal evolution of icy planetary interiors is not fully understood and its treatment is beyond the scope of this paper, however, if the ice layer is adiabatic, which likely corresponds to a lower bound for the temperature of the ices, they could host this carbon as organic molecules if temperature is insufficient for diamond formation (Figure 6), though this may lead to the conversion of methane to complex molecules (*Kolesnikov et al.*, 2009). Alternatively, processes such as tidal heating (*Scharf*, 2006) or radioactive heating can lead to high interior temperatures persisting at later times (*Bhatia and Sahijpal*, 2017). These processes may provide sufficient heating to sustain diamond formation over long timescales.

Thermal boundary layers in the planets could also lead to superadiabatic temperatures. The relevant thermal boundary layers would likely be either between a hot rocky mantle and the ices or a stagnant ice cap at the surface (*Deschamps*, 2021). The latter would act to trap heat within the planet, thus, raising the interior temperature. The former would occur if the chemical transition between rock and ice layers is discontinuous, however, the highest pressure ices, and thus those most likely to be able to precipitate diamond, occur at the bottom of the ice layer where it meets the rocky mantle. A hot, rocky mantle region would locally heat this ice and drive diamond precipitation near the interface.

Extreme temperatures can also result from a runaway greenhouse effect as the retention of a large portion of the stellar irradiance leads to high surface temperatures, which would slow cooling from internal heat sources. In this process, the water vapor-rich atmosphere retains stellar radiation, resulting in increased surface temperature and increased evaporation of the surface water, which in turn increases the temperature, leading to potentially extreme heating later in a planet's development (*Pierrehumbert*, 2023; *Boukrouche et al.*, 2021).

4 Effects on Icy Planets

Our results suggest that diamond precipitation is widespread in the ices of planets with high water content and radii greater than ∼0.75 times that of Earth where temperature is sufficient. Sinking of the denser diamond will lead to carbon depletion in the surface ices altering their chemistry. Material transport is expected within the ices and over time will bring an increasing portion of the carbon bearing ice to pressures where diamond formation can occur, resulting in the bulk depletion of carbon in the ice layer. Interior models of Uranus and Neptune, both larger than the planets considered here, generally assume convection in the ices (*Scheibe et al.*, 2019). Deeper within Uranus and Neptune large-scale convection of conductive ice has been proposed as an origin for their complex magnetic fields (*Stanley and Bloxham*, 2006). In smaller bodies, cryovolcanism is widespread on the icy moons of our solar system (*Fagents et al.*, 2022). This process ejects liquid water-rich material from the moon's interior, depositing it on the surface, burying that material, and over time transporting it deeper into the body. In either case, the viscosity of solid ice and liquid water is low for planets with sizes and temperatures investigated here, enabling convection within these layers over a wide range of thermal regimes (*Matusalem et al.*, 2022; *Abramson*, 2007; *Frost and Glenzer*, 2020; *Durham and Stern*, 2001).

Diamond formation results in the sequestration of carbon deeper within the planet and, where this depletes the surface carbon, the planet will be less favorable to carbon-based life. The astrobiological potential of both surface (*Kite and Ford*, 2018) and sub-surface (*Lipps et al.*, 2004) liquid water 'oceans' have been discussed. Liquid water is slightly denser than the ice Ih surface modeled here, but will convert to ice VI at 1 GPa, so the effect of such liquid oceans on the internal pressure of the planet would be small. Figure 3 shows the radius-mass relations for planets which do, and more importantly for astrobiology, do not, meet the conditions for diamond precipitation. Planets that cannot form diamonds in their icy mantles can be divided into two classes: those that are too small to generate enough pressure in the ices to allow for diamond formation, and those with low water content such that the thickness of the ice layer is insufficient to experience high pressures.

The first class of smaller planets and moons cannot have the surface carbon sequestered by diamond formation in their deep ices, meaning it will remain available in the surface ice. This is a factor which might favor astrobiology on icy bodies smaller than ~0.75 Earth radii. Small exoplanets are harder to detect, so it is uncertain how frequent these are beyond our solar system, as most fall below current detection limits. Locally, these are analogous to various icy moons, many of which are known to harbor complex carbon chemistry (*Hörst*, 2017; *Waite Jr et al.*, 2006) and the astrobiological potentials of which have been discussed at length (*Lipps et al.*, 2004; *Davila and Eigenbrode*, 2024; *Jebbar et al.*, 2020; *Cockell et al.*, 2024).

The second class corresponds to denser planets with compositions like that of a rocky planet with a thin surface water layer. Detection of these is likely to require spectroscopic techniques as the mean density change due to the ice can be small if the layer is thin and a similar density could be achieved via different compositions of the core and rocky mantle. Such data are currently sparse but results are to be expected in coming years (*Holmberg and Madhusudhan*, 2022; *Edwards et al.*, 2019). Unlike smaller icy bodies, there are no local planets fitting this category, however, the stronger volcanism expected in larger planets may enhance the impurity levels in the ices (*Luo et al.*, 2024b) and the lack of diamond precipitation in the ices means carbon can remain accessible to surface life.

In conclusion, we have modeled icy planets comprising an iron-silicon core, magnesium silicate lower mantle and icy upper mantle by self-consistently solving the hydrostatic equilibrium equation, which relates the density profile to the internal pressure due to gravity in a body in hydrostatic equilibrium, and the material equations of state of the layers. The results indicate that icy planets larger than ~0.75 Earth radii will exceed 10 GPa in the ice layer and thus can host diamond precipitation from carbon-containing molecules held within the ices. Planets massive enough to generate the required 10 GPa in the ices are expected to reach the 2000 K required for diamond formation from hydrocarbons shortly after accretion. This suggests that icy planets above ~0.75 Earth radii will have carbon-depleted ices as the diamond precipitation and subsequent subduction entraps the carbon deep within the planet. Carbon depletion of the surface ices has astrobiological implications, with reduced favourability for carbon-based life on an exoplanet.

Acknowledgements

The authors would like to thank Armin Bergermann for helpful discussions. This work was supported by US Department of Energy (DOE) Office of Fusion Energy Sciences FWP100866 award number DE-SCL0000130.

Author contributions

Conceptualization: MF; Software: AZ; Investigation and Methodology: AZ, EE, and MF; Supervision: SHG, and MF; the manuscript was written by AZ, EE and MF.

Data availability

The code used in this study can be found at https://github.com/AZhou0102/Diamond-Precipitation-Code.

Competing interests

The authors declare no conflicts of interest.

Copyright notice

References

Abramson, E. H. (2007), Viscosity of water measured to pressures of 6 GPa and temperatures of 300 °C, *Physical Review E*, *76*(5), 051,203, doi: http://doi.org/10.1103/PhysRevE.76.051203.

Akeson, R. L., X. Chen, D. Ciardi, M. Crane, J. Good, M. Harbut, E. Jackson, S. R. Kane, A. C. Laity, S. Leifer, et al. (2013), The NASA exoplanet archive: data and tools for exoplanet research, *Publications of the Astronomical Society of the Pacific*, *125*(930), 989, doi: http://doi.org/10.1086/672273.

Andrault, D., R. J. Angel, J. L. Mosenfelder, and T. Le Bihan (2003), Equation of state of stishovite to lower mantle pressures, *American Mineralogist*, *88*(2-3), 301–307, doi: http://doi.org/10.2138/am-2003-2-307.

Bailey, E., and D. J. Stevenson (2021), Thermodynamically governed interior models of Uranus and Neptune, *The Planetary Science Journal*, *2*(2), 64, doi: http://doi.org/10.3847/PSJ/abd1e0.

Baumeister, P., F. Miozzi, C. M. Guimond, M.-L. Steinmeyer, C. Dorn, S.-I. Karato, É. Bolmont, A. Revol, A. Thamm, and L. Noack (2025), Fundamentals of interior modelling and challenges in the interpretation of observed rocky exoplanets, *Space Science Reviews*, *221*(8), 123, doi: http://doi.org/10.1007/s11214-025-01248-5.

Benedetti, L. R., J. H. Nguyen, W. A. Caldwell, H. Liu, M. Kruger, and R. Jeanloz (1999), Dissociation of CH_4 at high pressures and temperatures: diamond formation in giant planet interiors?, *Science*, *286*(5437), 100–102, doi: http://doi.org/10.1126/science.286.5437.100.

Bergermann, A., M. French, and R. Redmer (2024), Ab initio calculation of the miscibility diagram for mixtures of hydrogen and water, *Physical Review B*, *109*(17), 174,107, doi: http://doi.org/10.1103/PhysRevB.109.174107.

Bethkenhagen, M., E. R. Meyer, S. Hamel, N. Nettelmann, M. French, L. Scheibe, C. Ticknor, L. A. Collins, J. D. Kress, J. J. Fortney, et al. (2017), Planetary ices and the linear mixing approximation, *The Astrophysical Journal*, *848*(1), 67, doi: http://doi.org/10.3847/1538-4357/aa8b14.

Bezacier, L., B. Journaux, J.-P. Perrillat, H. Cardon, M. Hanfland, and I. Daniel (2014), Equations of state of ice VI and ice VII at high pressure and high temperature, *The Journal of Chemical Physics*, *141*(10), 104,505, doi: http://doi.org/10.1063/1.4894421.

Bhatia, G. K., and S. Sahijpal (2017), Thermal evolution of trans-Neptunian objects, icy satellites, and minor icy planets in the early solar system, *Meteoritics & Planetary Science*, *52*(12), 2470–2490, doi: http://doi.org/10.1111/maps.12952.

Bonati, I., M. Lasbleis, and L. Noack (2021), Structure and thermal evolution of exoplanetary cores, *Journal of Geophysical Research: Planets*, *126*(5), e2020JE006,724, doi: http://doi.org/10.1029/2020JE006724.

Bottke, W. F., and M. D. Norman (2017), The late heavy bombardment, *Annual Review of Earth and Planetary Sciences*, *45*(1), 619–647, doi: http://doi.org/10.1146/annurev-earth-063016-020131.

Boukrouche, R., T. Lichtenberg, and R. T. Pierrehumbert (2021), Beyond runaway: initiation of the post-runaway greenhouse state on rocky exoplanets, *The Astrophysical Journal*, *919*(2), 130, doi: http://doi.org/10.3847/1538-4357/ac1345.

Cano Amoros, M., N. Nettelmann, N. Tosi, P. Baumeister, and H. Rauer (2024), H2–H2O demixing in Uranus and Neptune: Adiabatic structure models, *Astronomy & Astrophysics*, *692*, A152, doi: http://doi.org/10.1051/0004-6361/202452148.

Cheng, B., S. Hamel, and M. Bethkenhagen (2023), Thermodynamics of diamond formation from hydrocarbon mixtures in planets, *Nature Communications*, *14*(1), 1104, doi: http://doi.org/10.1038/s41467-023-36841-1.

Christiansen, J. (2018), *Exoplanet Catalogs*, pp. 1933–1947, Springer International Publishing, Cham, doi: http://doi.org/10.1007/978-3-319-55333-7_150.

Cockell, C. S. (2020), *Astrobiology: understanding life in the universe*, 2nd edition ed., Wiley-Blackwell.

Cockell, C. S., M. Simons, J. Castillo-Rogez, P. M. Higgins, L. Kaltenegger, J. T. Keane, E. J. Leonard, K. L. Mitchell, R. S. Park, S. M. Perl, et al. (2024), Sustained and comparative habitability beyond Earth, *Nature Astronomy*, *8*(1), 30–38, doi: http://doi.org/10.1038/s41550-023-02158-8.

Davila, A. F., and J. L. Eigenbrode (2024), Enceladus: Astrobiology Revisited, *Journal of Geophysical Research: Biogeosciences*, *129*(5), e2023JG007,677, doi: http://doi.org/10.1029/2023JG007677.

Deschamps, F. (2021), Stagnant lid convection with temperature-dependent thermal conductivity and the thermal evolution of icy worlds, *Geophysical Journal International*, *224*(3), 1870–1889, doi: http://doi.org/10.1093/gji/ggaa540.

Dorn, C., and T. Lichtenberg (2021), Hidden water in magma ocean exoplanets, *The Astrophysical Journal Letters*, *922*(1), L4, doi: http://doi.org/10.3847/2041-8213/ac33af.

Dorn, C., J. Venturini, A. Khan, K. Heng, Y. Alibert, R. Helled, A. Rivoldini, and W. Benz (2016), A generalized Bayesian inference method for constraining the interiors of super Earths and sub-Neptunes, *Astronomy & Astrophysics*, *597*, A37, doi: http://doi.org/10.1051/0004-6361/201628708.

Downs, R. T., C.-S. Zha, T. S. Duffy, and L. W. Finger (1996), The equation of state of forsterite to 17.2 GPa and effects of pressure media, *American Mineralogist*, *81*(1-2), 51–55, doi: http://doi.org/10.2138/am-1996-1-207.

Durham, W. B., and L. A. Stern (2001), Rheological properties of water ice—Applications to satellites of the outer planets, *Annual Review of Earth and Planetary Sciences*, *29*(1), 295–330, doi: http://doi.org/10.1146/annurev.earth.29.1.295.

Edwards, B., M. Rice, T. Zingales, M. Tessenyi, I. Waldmann, G. Tinetti, E. Pascale, G. Savini, and S. Sarkar (2019), Exoplanet spectroscopy and photometry with the Twinkle space telescope, *Experimental Astronomy*, *47*, 29–63, doi: http://doi.org/10.1007/s10686-018-9611-4.

Elkins-Tanton, L. T. (2012), Magma oceans in the inner solar system, *Annual Review of Earth and Planetary Sciences*, *40*(1), 113–139, doi: http://doi.org/10.1146/annurev-earth-042711-105503.

Fagents, S. A., R. M. C. Lopes, L. C. Quick, and T. K. P. Gregg (2022), Cryovolcanism, in *Planetary volcanism across the solar System*, *Comparative Planetology*, vol. 1, edited by T. K. Gregg, R. M. Lopes, and S. A. Fagents, pp. 161–234, Elsevier, doi: http://doi.org/10.1016/B978-0-12-813987-5.00005-5.

Fiquet, G., D. Andrault, A. Dewaele, T. Charpin, M. Kunz, and D. Haüsermann (1998), PVT equation of state of $MgSiO_3$ perovskite, *Physics of the Earth and Planetary Interiors*, *105*(1-2), 21–31, doi: http://doi.org/10.1016/S0031-9201(97)00077-0.

Frost, M., and S. H. Glenzer (2020), Isotope effects on the high pressure viscosity of liquid water measured by differential dynamic microscopy, *Applied Physics Letters*, *116*(23), 233,701, doi: http://doi.org/10.1063/5.0012750.

Frost, M., R. S. McWilliams, E. Bykova, M. Bykov, R. J. Husband, L. M. Andriambariarijaona, S. Khandarkhaeva, B. Massani, K. Appel, C. Baehtz, et al. (2024), Diamond precipitation dynamics from hydrocarbons at icy planet interior conditions, *Nature Astronomy*, *8*(2), 174–181, doi: http://doi.org/10.1038/s41550-023-02147-x.

Frost, M., M. A. Kuzovnikov, P. Dalladay-Simpson, R. T. Howie, J. S.

Loveday, U. Ranieri, and E. Gregoryanz (2025), Implications of high-pressure oxygen hydrates on radiolytic oxygen in Jovian icy moons, *Communications Chemistry*, *8*(128), doi: http://doi.org/10.1038/s42004-025-01509-y.

Greene, T. P., M. R. Line, C. Montero, J. J. Fortney, J. Lustig-Yaeger, and K. Luther (2016), Characterizing transiting exoplanet atmospheres with JWST, *The Astrophysical Journal*, *817*(1), 17, doi: http://doi.org/10.3847/0004-637X/817/1/17.

Haldemann, J., Y. Alibert, C. Mordasini, and W. Benz (2020), AQUA: a collection of H2O equations of state for planetary models, *Astronomy & Astrophysics*, *643*, A105, doi: http://doi.org/10.1051/0004-6361/202038367.

Haldemann, J., V. Ksoll, D. Walter, Y. Alibert, R. S. Klessen, W. Benz, U. Koethe, L. Ardizzone, and C. Rother (2023), Exoplanet characterization using conditional invertible neural networks, *Astronomy & Astrophysics*, *672*, A180, doi: http://doi.org/10.1051/0004-6361/202243230.

Hanks, T. C., and D. L. Anderson (1969), The early thermal history of the Earth, *Physics of the Earth and Planetary Interiors*, *2*(1), 19–29, doi: http://doi.org/10.1016/0031-9201(69)90015-6.

Hazen, R. M., J. Zhang, and J. Ko (1990), Effects of Fe/Mg on the compressibility of synthetic wadsleyite: β-$(Mg_{1-x}Fe_x)_2SiO_4$ (x<0.25), *Physics and Chemistry of Minerals*, *17*(5), 416–419, doi: http://doi.org/10.1007/BF00212210.

Hirai, H., K. Konagai, T. Kawamura, Y. Yamamoto, and T. Yagi (2009), Polymerization and diamond formation from melting methane and their implications in ice layer of giant planets, *Physics of the Earth and Planetary Interiors*, *174*(1-4), 242–246, doi: http://doi.org/10.1016/j.pepi.2008.06.011.

Hirose, K., B. Wood, and L. Vočadlo (2021), Light elements in the Earth's core, *Nature Reviews Earth & Environment*, *2*(9), 645–658, doi: http://doi.org/10.1038/s43017-021-00203-6.

Holmberg, M., and N. Madhusudhan (2022), A First Look at CRIRES+: Performance Assessment and Exoplanet Spectroscopy, *The Astronomical Journal*, *164*(3), 79, doi: http://doi.org/10.3847/1538-3881/ac77eb.

Horedt, G. P. (1980), Gravitational heating of planets, *Physics of the Earth and Planetary Interiors*, *21*(1), 22–30, doi: http://doi.org/10.1016/0031-9201(80)90016-3.

Hörst, S. M. (2017), Titan's atmosphere and climate, *Journal of Geophysical Research: Planets*, *122*(3), 432–482, doi: http://doi.org/10.1002/2016JE005240.

Howard, S., S. Müller, and R. Helled (2024), Evolution of Jupiter and Saturn with helium rain, *Astronomy & Astrophysics*, *689*, A15, doi: http://doi.org/10.1051/0004-6361/202450629.

Howard, S., R. Helled, A. Bergermann, and R. Redmer (2025), The possibility of hydrogen-water demixing in Uranus, Neptune, K2-18 b and TOI-270 d, *Astronomy & Astrophysics*, *703*, A154, doi: http://doi.org/10.1051/0004-6361/202556322.

Jebbar, M., K. Hickman-Lewis, B. Cavalazzi, R.-S. Taubner, S. K.-M. R. Rittmann, and A. Antunes (2020), Microbial diversity and biosignatures: an icy moons perspective, *Space Science Reviews*, *216*(1), 10, doi: http://doi.org/10.1007/s11214-019-0620-z.

Kadobayashi, H., H. Hirai, H. Ohfuji, M. Ohtake, M. Muraoka, S. Yoshida, and Y. Yamamoto (2020), Structural evolution of methane hydrate under pressures up to 134 GPa, *The Journal of Chemical Physics*, *152*(19), doi: http://doi.org/10.1063/5.0007511.

Kadobayashi, H., S. Ohnishi, H. Ohfuji, Y. Yamamoto, M. Muraoka, S. Yoshida, N. Hirao, S. Kawaguchi-Imada, and H. Hirai (2021), Diamond formation from methane hydrate under the internal conditions of giant icy planets, *Scientific Reports*, *11*(1), 8165, doi: http://doi.org/10.1038/s41598-021-87638-5.

Kite, E. S., and E. B. Ford (2018), Habitability of exoplanet waterworlds, *The Astrophysical Journal*, *864*(1), 75, doi: http://doi.org/10.3847/1538-4357/aad6e0.

Klotz, S., L. E. Bove, T. Strässle, T. C. Hansen, and A. M. Saitta (2009), The preparation and structure of salty ice VII under pressure, *Nature Materials*, *8*(5), 405–409, doi: http://doi.org/10.1038/nmat2422.

Kobayashi, C., A. I. Karakas, and M. Lugaro (2020), The origin of elements from carbon to uranium, *The Astrophysical Journal*, *900*(2), 179, doi: http://doi.org/10.3847/1538-4357/abae65.

Kolesnikov, A., V. G. Kutcherov, and A. F. Goncharov (2009), Methane-derived hydrocarbons produced under upper-mantle conditions, *Nature Geoscience*, *2*(8), 566–570, doi: http://doi.org/10.1038/ngeo591.

Kovačević, T., F. González-Cataldo, S. T. Stewart, and B. Militzer (2022), Miscibility of rock and ice in the interiors of water worlds, *Scientific Reports*, *12*(1), 13,055, doi: http://doi.org/10.1038/s41598-022-16816-w.

Kraus, D., J. Vorberger, A. Pak, N. J. Hartley, L. B. Fletcher, S. Frydrych, E. Galtier, E. J. Gamboa, D. O. Gericke, S. H. Glenzer, et al. (2017), Formation of diamonds in laser-compressed hydrocarbons at planetary interior conditions, *Nature Astronomy*, *1*(9), 606–611, doi: http://doi.org/10.1038/s41550-017-0219-9.

Lai, X., F. Zhu, D. Zhang, S. Tkachev, V. B. Prakapenka, K.-H. Chao, and B. Chen (2023), Thermal equation of state of ice-VII revisited by single-crystal X-ray diffraction, *American Mineralogist*, *108*(8), 1530–1537, doi: http://doi.org/10.2138/am-2022-8554.

Levien, L., and C. T. Prewitt (1981), High-pressure crystal structure and compressibility of coesite, *American Mineralogist*, *66*(3-4), 324–333.

Lin, Y., R. E. Cohen, S. Stackhouse, K. P. Driver, B. Militzer, L. Shulenburger, and J. Kim (2014), Equations of state and stability of $MgSiO_3$ perovskite and post-perovskite phases from quantum Monte Carlo simulations, *Physical Review B*, *90*(18), 184,103, doi: http://doi.org/10.1103/PhysRevB.90.184103.

Lipps, J. H., G. Delory, J. T. Pitman, and S. Rieboldt (2004), Astrobiology of Jupiter's icy moons, in *Instruments, Methods, and Missions for Astrobiology VIII*, vol. 5555, pp. 78–92, SPIE, doi: http://doi.org/10.1117/12.560356.

Litasov, K. D., and A. F. Shatskiy (2016), Composition of the Earth's core: A review, *Russian Geology and Geophysics*, *57*(1), 22–46, doi: http://doi.org/10.1016/j.rgg.2016.01.003.

Lobanov, S. S., P.-N. Chen, X.-J. Chen, C.-S. Zha, K. D. Litasov, H.-K. Mao, and A. F. Goncharov (2013), Carbon precipitation from heavy hydrocarbon fluid in deep planetary interiors, *Nature Communications*, *4*(1), 2446, doi: http://doi.org/10.1038/ncomms3446.

Loveday, J. S., R. J. Nelmes, M. Guthrie, S. A. Belmonte, D. R.

Allan, D. D. Klug, J. S. Tse, and Y. P. Handa (2001), Stable methane hydrate above 2 GPa and the source of Titan's atmospheric methane, *Nature*, *410*(6829), 661–663, doi: http://doi.org/10.1038/35070513.

Luo, H., C. Dorn, and J. Deng (2024a), The interior as the dominant water reservoir in super-Earths and sub-Neptunes, *Nature Astronomy*, *8*(11), 1399–1407, doi: http://doi.org/10.1038/s41550-024-02347-z.

Luo, H., J. G. O'Rourke, and J. Deng (2024b), Radiogenic heating sustains long-lived volcanism and magnetic dynamos in super-Earths, *Science Advances*, *10*(37), eado7603, doi: http://doi.org/10.1126/sciadv.ado7603.

Madhusudhan, N., A. A. Piette, and S. Constantinou (2021), Habitability and biosignatures of hycean worlds, *The Astrophysical Journal*, *918*(1), 1, doi: http://doi.org/10.3847/1538-4357/abfd9c.

Marboeuf, U., O. Mousis, D. Ehrenreich, Y. Alibert, A. Cassan, V. Wakelam, and J.-P. Beaulieu (2008), Composition of ices in low-mass extrasolar planets, *The Astrophysical Journal*, *681*(2), 1624, doi: http://doi.org/10.1086/588777.

Matusalem, F., J. Santos Rego, and M. de Koning (2022), Plastic deformation of superionic water ices, *Proceedings of the National Academy of Sciences*, *119*(45), e2203397,119, doi: http://doi.org/10.1073/pnas.2203397119.

Mayor, M., and D. Queloz (1995), A Jupiter-mass companion to a solar-type star, *Nature*, *378*(6555), 355–359, doi: http://doi.org/10.1038/378355a0.

McDonough, W. F., and S.-S. Sun (1995), The composition of the Earth, *Chemical Geology*, *120*(3-4), 223–253, doi: http://doi.org/10.1016/0009-2541(94)00140-4.

Meng, Y., Y. Fei, D. J. Weidner, G. D. Gwanmesia, and J. Hu (1994), Hydrostatic compression of γ-Mg_2SiO_4 to mantle pressures and 700 K: Thermal equation of state and related thermoelastic properties, *Physics and Chemistry of Minerals*, *21*, 407–412, doi: http://doi.org/10.1007/BF00203299.

Mondal, A., R. J. Husband, H.-P. Liermann, and C. Sanchez-Valle (2023), Equation of state of ammonia dihydrate up to 112 GPa by static and dynamic compression experiments in diamond anvil cells, *Physical Review B*, *107*(22), 224,108, doi: http://doi.org/10.1103/PhysRevB.107.224108.

Naden Robinson, V., Y. Wang, Y. Ma, and A. Hermann (2017), Stabilization of ammonia-rich hydrate inside icy planets, *Proceedings of the National Academy of Sciences*, *114*(34), 9003–9008, doi: http://doi.org/10.1073/pnas.1706244114.

Otegi, J. F., C. Dorn, R. Helled, F. Bouchy, J. Haldemann, and Y. Alibert (2020), Impact of the measured parameters of exoplanets on the inferred internal structure, *Astronomy & Astrophysics*, *640*, A135, doi: http://doi.org/10.1051/0004-6361/202038006.

Pearson, V. K., M. A. Sephton, I. A. Franchi, J. M. Gibson, and I. Gilmour (2006), Carbon and nitrogen in carbonaceous chondrites: Elemental abundances and stable isotopic compositions, *Meteoritics & Planetary Science*, *41*(12), 1899–1918, doi: http://doi.org/10.1111/j.1945-5100.2006.tb00459.x.

Pierrehumbert, R. T. (2023), The runaway greenhouse on sub-Neptune waterworlds, *The Astrophysical Journal*, *944*(1), 20, doi: http://doi.org/10.3847/1538-4357/acafdf.

Ransford, G. A. (1982), The accretional heating of the terrestrial planets: a review, *Physics of the Earth and Planetary Interiors*, *29*(3-4), 209–217, doi: http://doi.org/10.1016/0031-9201(82)90012-7.

Rigby, F. E., and N. Madhusudhan (2024), On the ocean conditions of Hycean worlds, *Monthly Notices of the Royal Astronomical Society*, *529*(1), 409–424, doi: http://doi.org/10.1093/mnras/stae413.

Rogers, L. A., and S. Seager (2010), A framework for quantifying the degeneracies of exoplanet interior compositions, *The Astrophysical Journal*, *712*(2), 974, doi: http://doi.org/10.1088/0004-637X/712/2/974.

Roy, A. J., M. Bethkenhagen, A. Bergermann, and R. Redmer (2025), Understanding the Transport Properties of Methane–Hydrogen Mixtures under the Interior Conditions of Ice Giants, *The Astrophysical Journal*, *990*(2), 212, doi: http://doi.org/10.3847/1538-4357/adf5be.

Scharf, C. A. (2006), The potential for tidally heated icy and temperate moons around exoplanets, *The Astrophysical Journal*, *648*(2), 1196, doi: http://doi.org/10.1086/505256.

Scheibe, L., N. Nettelmann, and R. Redmer (2019), Thermal evolution of Uranus and Neptune-I. Adiabatic models, *Astronomy & Astrophysics*, *632*, A70, doi: http://doi.org/10.1051/0004-6361/201936378.

Schöttler, M., and R. Redmer (2018), Ab initio calculation of the miscibility diagram for hydrogen-helium mixtures, *Physical Review Letters*, *120*(11), 115,703, doi: http://doi.org/10.1103/PhysRevLett.120.115703.

Schubert, G., and T. Spohn (1990), Thermal history of Mars and the sulfur content of its core, *Journal of Geophysical Research: Solid Earth*, *95*(B9), 14,095–14,104, doi: http://doi.org/10.1029/JB095iB09p14095.

Schuster, A. K., N. J. Hartley, J. Vorberger, T. Döppner, T. Van Driel, R. W. Falcone, L. B. Fletcher, S. Frydrych, E. Galtier, E. J. Gamboa, et al. (2020), Measurement of diamond nucleation rates from hydrocarbons at conditions comparable to the interiors of icy giant planets, *Physical Review B*, *101*(5), 054,301, doi: http://doi.org/10.1103/PhysRevB.101.054301.

Spiegel, D. S., J. J. Fortney, and C. Sotin (2014), Structure of exoplanets, *Proceedings of the National Academy of Sciences*, *111*(35), 12,622–12,627, doi: http://doi.org/10.1073/pnas.1304206111.

Stanley, S., and J. Bloxham (2006), Numerical dynamo models of Uranus' and Neptune's magnetic fields, *Icarus*, *184*(2), 556–572, doi: http://doi.org/10.1016/j.icarus.2006.05.005.

Strässle, T., S. Klotz, J. S. Loveday, and M. Braden (2005), Equation of state of ordinary ice Ih at 145 K under true hydrostatic pressure up to 5 kbar, *Journal of Physics: Condensed Matter*, *17*(40), S3029, doi: http://doi.org/10.1088/0953-8984/17/40/006.

Szalay, J. R., F. Allegrini, R. W. Ebert, F. Bagenal, S. J. Bolton, S. Fatemi, D. J. McComas, A. Pontoni, J. Saur, H. T. Smith, et al. (2024), Oxygen production from dissociation of Europa's water-ice surface, *Nature astronomy*, pp. 1–10, doi: http://doi.org/10.1038/s41550-024-02206-x.

Teanby, N. A., P. G. J. Irwin, J. I. Moses, and R. Helled (2020), Neptune and Uranus: ice or rock giants?, *Philosophical Transactions of the Royal Society A*, *378*(2187), 20190,489, doi:

http://doi.org/10.1098/rsta.2019.0489.

Tjoa, J. N. K. Y., M. Mueller, and F. F. S. van der Tak (2020), The subsurface habitability of small, icy exomoons, *Astronomy & Astrophysics*, *636*, A50, doi: http://doi.org/10.1051/0004-6361/201937035.

Unterborn, C. T., and W. R. Panero (2019), The pressure and temperature limits of likely rocky exoplanets, *Journal of Geophysical Research: Planets*, *124*(7), 1704–1716, doi: http://doi.org/10.1029/2018JE005844.

Van Hoolst, T., L. Noack, and A. Rivoldini (2019), Exoplanet interiors and habitability, *Advances in Physics: X*, *4*(1), 1630,316, doi: http://doi.org/10.1080/23746149.2019.1630316.

Waite Jr, J. H., M. R. Combi, W.-H. Ip, T. E. Cravens, R. L. McNutt Jr, W. Kasprzak, R. Yelle, J. Luhmann, H. Niemann, D. Gell, et al. (2006), Cassini ion and neutral mass spectrometer: Enceladus plume composition and structure, *Science*, *311*(5766), 1419–1422, doi: http://doi.org/10.1126/science.1121290.

Wang, J., Z. Mao, F. Jiang, and T. S. Duffy (2015), Elasticity of single-crystal quartz to 10 GPa, *Physics and Chemistry of Minerals*, *42*, 203–212, doi: http://doi.org/10.1007/s00269-014-0711-z.

Wang, Z., and H. Becker (2013), Ratios of S, Se and Te in the silicate Earth require a volatile-rich late veneer, *Nature*, *499*(7458), 328–331, doi: http://doi.org/10.1038/nature12285.

Wicks, J. K., R. F. Smith, D. E. Fratanduono, F. Coppari, R. G. Kraus, M. G. Newman, J. R. Rygg, J. H. Eggert, and T. S. Duffy (2018), Crystal structure and equation of state of Fe-Si alloys at super-Earth core conditions, *Science Advances*, *4*(4), eaao5864, doi: http://doi.org/10.1126/sciadv.aao5864.

Wolanin, E., P. Pruzan, J. C. Chervin, B. Canny, M. Gauthier, D. Häusermann, and M. Hanfland (1997), Equation of state of ice VII up to 106 GPa, *Physical Review B*, *56*(10), 5781, doi: http://doi.org/10.1103/PhysRevB.56.5781.

Zeng, L., S. B. Jacobsen, D. D. Sasselov, M. I. Petaev, A. Vanderburg, M. Lopez-Morales, J. Perez-Mercader, T. R. Mattsson, G. Li, M. Z. Heising, et al. (2019), Growth model interpretation of planet size distribution, *Proceedings of the National Academy of Sciences*, *116*(20), 9723–9728, doi: http://doi.org/10.1073/pnas.1812905116.